CHIN. PHYS. LETT. Vol. 38, No. 3 (2021) 034201

Ultra-Broadband Infrared Metamaterial Absorber for Passive Radiative Cooling

Yan-Ning Liu(刘彦宁)[1,2], Xiao-Long Weng(翁小龙)[1,2], Peng Zhang(张澎)[3*], Wen-Xin Li(李文新)[1,2], Yu Gong(宫禹)[3], Li Zhang(张丽)[1,2], Tian-Cheng Han(韩天成)[1,2], Pei-Heng Zhou(周佩珩)[1,2], and Long-Jiang Deng(邓龙江)[1,2*]

[1]*National Engineering Research Center of Electromagnetic Radiation Control Materials, University of Electronic Science and Technology of China, Chengdu 611731, China*
[2]*Key Laboratory of Multi-spectral Absorbing Materials and Structures of Ministry of Education, University of Electronic Science and Technology of China, Chengdu 611731, China*
[3]*Shenyang Aircraft Design and Research Institute, Shenyang 110035, China*

(Received 7 October 2020; accepted 5 January 2021; published online 2 March 2021)

Infrared metamaterial absorber (MMA) based on metal-insulator-metal (MIM) configuration with flexible design, perfect and selective absorption, has attracted much attention recently for passive radiative cooling applications. To cool objects passively, broadband infrared absorption (i.e. 8–14 μm) is desirable to emit thermal energy through atmosphere window. We present a novel MMA composed of multilayer MIM resonators periodically arranged on a PbTe/MgF_2 bilayer substrate. Verified by the rigorous coupled-wave analysis method, the proposed MMA shows a relative bandwidth of about 45% (from 8.3 to 13.1 μm with the absorption intensity over 0.8). The broadband absorption performs stably over a wide incident angle range (below 50°) and predicts 12 K cooling below ambient temperature at nighttime. Compared with the previous passive radiative coolers, our design gets rid of the continuous metal substrate and provides an almost ideal transparency window (close to 100%) for millimeter waves over 1 mm. The structure is expected to have potential applications in thermal control of integrated devices, where millimeter wave signal compatibility is also required.

DOI: 10.1088/0256-307X/38/3/034201

Objects at any temperatures above absolute zero can radiate energy.[1] As the temperature of outer space (3 K) is far below the objects on earth [e.g., our body (310 K)], it is impossible to ignore the heat exchange between these two resources.[2] Other than this remarkable temperature difference, the perfect transparency window of earth's atmosphere (8–14 μm) for infrared radiation[3] ensures that the heat radiates straightly through this window to the icy outer space without any block. Thus, the passive radiative coolers, which make use of this radiation process to cool themselves down, are called energy-saving materials.[4–6] Thermal emission spectra of the coolers, or infrared absorption spectra according to Kirchhoff's law, acts predominantly to determine the cooling efficiency. Strong, broadband and highly selective spectra are mostly pursued by researchers.[7] Meanwhile, the fast developments in nanostructure/thin film fabrication techniques make it more and more convenient to manipulate material properties artificially.[1,2] Till now, photonic crystals,[8–10] nanoparticles[11–14] and metamaterials[15–17] are the most researched infrared selective emission materials. A nanoparticle-blended polymer film is one of the most feasible forms of passive coolers, but its spectral selectivity is limited by random blending. Multilayer systems require complex design and elaborate fabrication of variant thin films,[18] especially for those of infrared properties sensitive to thickness.[1]

Therefore, metamaterials, which possess perspective advantages of thin thickness, high design flexibility, matured fabrication process and near-ideal selective emissive spectrum,[19] have been proved to be a more promising candidate. Metamaterial absorber (MMA) is one of the most important branches of metamaterials, which absorbs the incident wave energy efficiently.[20] In 2008, MMA was firstly demonstrated by Landy *et al.*[21] in the microwave regime by periodic arrays of 2D electric ring resonators. Till now, MMA has been developed rapidly in applications of radar cross section (RCS) reduction, detection and sensors, and selective thermal emitters.[22,23] For selective thermal emitters, metal-insulator-metal (MIM) structure is one of the mostly adopted configurations.[24–27] The MIM resonators are usually composed of three layers: periodical arrays of meta-atom on the top, a continuous metallic plate on the bottom and a dielec-

Supported by the National Natural Science Foundation of China (Grant Nos. 52022018 and 52021001), and the Program for Changjiang Scholars and Innovative Research Team in University.
*Corresponding authors. Email: denglj@uestc.edu.cn; 13998189002@163.com
© 2021 Chinese Physical Society and IOP Publishing Ltd

tric spacer in the middle. The continuous metallic ground plate eliminates wave transmittance and thus enhances absorption inside the absorber. A single layer of MIM resonators has been used to realize near-ideal and strictly selective absorption in infrared, but with relatively narrow bandwidth.[25] Many efforts have been made for this issue, e.g. stacking multilayers of MIM units,[28–30] combining several top metaatom patterns in a unit[31,32] or loading lossy materials inside.[33,34] As far as the application of passive radiative cooling is considered, Hossain *et al.* have proposed kinds of MIM-based broadband radiative coolers which have strong absorption over a wide incident angle range in the atmosphere radiation window of 8–14 μm, and the passive cooling devices they designed can lower temperature by 10 K below ambient temperature.[19,35] However, it should be noted that in practical applications for thermal emission control where wireless communication is also necessary, the MIM-based MMA is limited by wireless signal shielding effect of the continuous metallic plate in the MIM structure.

In this study, we propose a highly selective and ultra-broadband metamaterial absorber for passive radiative cooling applications. Our design is based on the stacking of four MIM subwavelength units, as the continuous metallic plate of the traditional MIM absorbers is replaced with a PbTe/MgF_2 bilayer dielectric substrate to solve the wireless signal shielding problem. The broadband absorption that covers exactly the atmosphere window is achieved with a small thickness (1.35 μm). Using the rigorous coupled-wave analysis (RCWA) method, a relative bandwidth of over 45% (ranging from 8.3 to 13.1 μm) for absorption intensity over 0.8 is verified. Furthermore, our absorber shows the near-ideal transparency for wireless signals.

As mentioned above, the MIM structure has been extensively used in MMAs because of its simple configuration. Here, we also begin with an MIM structure, named by unit 1. As shown in Fig. 1(a), Al film (describe as the Drude model,[36] with plasma frequency $\omega_p = 1.24 \times 10^{16}$ rad·s^{-1} and damping constant $\Gamma = 2.24 \times 10^{14}$ s^{-1}) acts as the top and bottom metal layers and MgF_2 film ($\varepsilon_r = 1.74$) is sandwiched in the middle. When illuminated by TM normal incident light (the electric field is polarized along the X axis), there exists a near-ideal absorption peak at 8.1 μm (MRA1, as MRA is short for magnetic resonance absorption) but with narrow bandwidth [shown in Fig. 1(b)]. According to the equivalent circuit model of magnetic resonance[37] [see the inset in Fig. 1(b)], the resonance wavelength can be estimated by $\lambda_m = 2\pi b\sqrt{\varepsilon_r m_1}/2$ (the factor $m_1 = 0.25$ in this article).[38] The calculated result of $\lambda_m = 8.1$ is precisely consistent with the RCWA and CST simulation results. The mechanism of MRA1 is therefore verified as the intrinsic mode of magnetic resonance in MIM resonators.

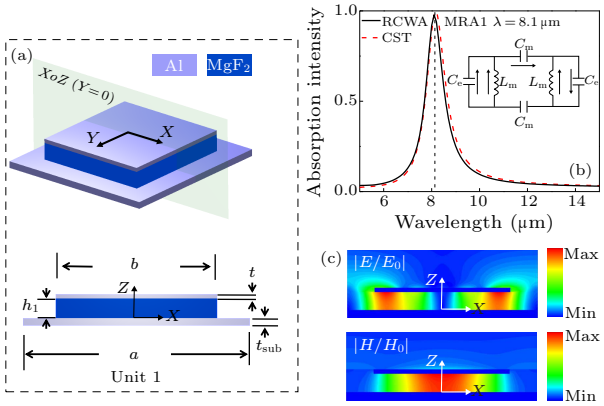

Fig. 1. (a) Schematic diagram of the single MIM resonator unit 1. The period and the length of unit 1 are set as $a = 3.8$ μm and $b = 2.7$ μm, while other parameters are $h_1 = 0.2$ μm for the thickness of dielectric film, $t = 0.05$ μm for the thickness of top Al film and $t_{sub} = 0.1$ μm for the thickness of Al substrate. (b) Simulated absorption spectra with an inset of equivalent circuit for unit 1 under TM incidence. The absorption spectra are simulated by both RCWA method and the commercial CST software. The boundaries are selected as unit cells in X and Y directions, and open (add space) in Z direction. (c) Distributions of the electric and magnetic field for unit 1 at resonance wavelength of 8.1 μm as simulated by the RCWA method.

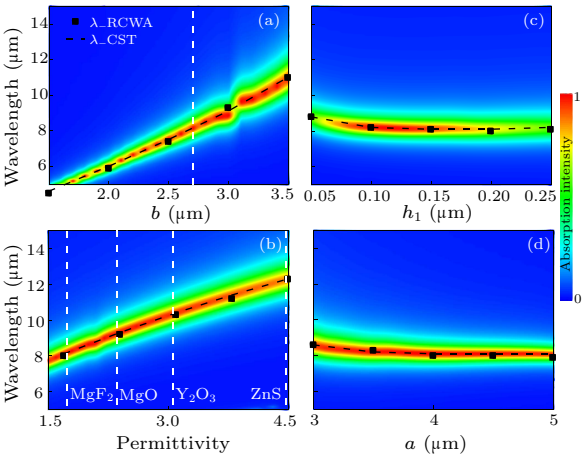

Fig. 2. Absorption diagram for unit 1 as a function of (a) the resonator length b [with $a = 3.8$ μm, $h_1 = 0.2$ μm, and the dielectric $MgF_2(\varepsilon_r = 1.74)$], (b) the permittivity of the dielectric layer (with $a = 3.8$ μm, $b = 2.7$ μm, and $h_1 = 0.2$ μm), (c) the thickness of the dielectric layer h_1 [with $a = 3.8$ μm, $b = 2.7$ μm, and the dielectric $MgF_2(\varepsilon_r = 1.74)$] and (d) the periodic of the resonator a [with $b = 2.7$ μm, $h_1 = 0.2$ μm, and the dielectric $MgF_2(\varepsilon_r = 1.74)$].

Furthermore, the magnetic resonance mode can also be confirmed by the electric and magnetic (EM) field profiles revealed in Fig. 1(c). According to the cross-sectional image of EM fields, a typical feature of magnetic resonance in MIM is shown: with H_y con-

centrated in the middle of the dielectric layer and with E_z restricted around the two sides of the resonator inside dielectric layer ($x = -b/2$ and $x = b/2$).

To understand how the structural or materials parameters affects the absorption of MIM resonators, we investigate four main parameters (b, *permittivity*, h_1 and a) by the absorption diagrams mapped in Fig. 2. Figure 2(a) presents the influence of the resonator length b: with the length increasing from 1.5 μm to 3.5 μm, the absorption peaks redshift gradually along the slant line approximately, while the intensity is stable around the near-ideal value. The absorption peak of unit 1 shifts to 8 μm as b approaches to 2.7 μm. For the effect of the permittivity of dielectric layer shown in Fig. 2(b), the absorption peak shifts towards large wavelengths as the permittivity increases from 1.5 to 4.5, and the intensity drops slightly. These two factors act as the primary adjusting parameters for absorption peaks while regardless of the intensity. Next, we study the thickness of dielectric layer h_1. As shown in Fig. 2(c), the absorption intensity is affected obviously by h_1, while the absorption peak is rarely shifted. This means that the thickness acts as an optimizing parameter to regulate absorption intensity on demand. Finally, for the period a of our unit 1, the absorption peak is weakly affected [see Fig. 2(d)], indicating strong localization of resonances inside the resonator [as can be proved in Fig. 1(c)].

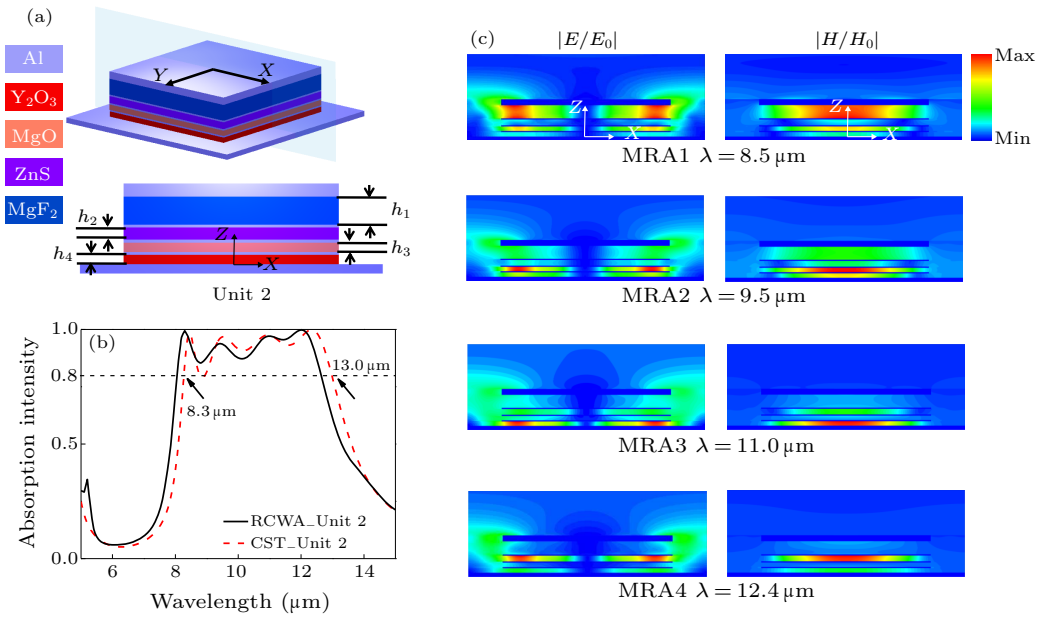

Fig. 3. (a) Schematic diagram of the resonator unit 2 composed of four overlapped MIM resonators. The value of a, b, t_{sub} are all equal to those of unit 1, while other parameters of dielectric layers are $h_1 = 0.3$ μm for MgF_2, $h_2 = 0.13$ μm for ZnS, $h_3 = 0.1$ μm for MgO, $h_4 = 0.1$ μm for Y_2O_3, 0.14 μm of the thickness of top Al plate, 0.03 μm for the thicknesses of other Al metal plates in the middle, and $t_{sub} = 0.1$ μm. (b) Simulated absorption spectra of unit 2. (c) Distribution of the electric/magnetic field for unit 2 numerical obtained by the RCWA method at four MRA wavelengths.

Here, our broadband design strategies are inherited from pervious works,[30,35,39] which implies that the stacking of MIM resonators results in the overlap of resonance absorption peaks. Firstly, we choose the same resonator length $b = 2.7$ μm, period $a = 3.8$ μm and thickness $h_1 = 0.2$ μm for each of the MIM resonators according to the parameter analysis of unit 1. Then the four dielectrics for MIM resonators are selected as shown in Fig. 2(b), and their absorption peaks span from 8 μm to 12 μm. These peaks are spectrally separated, with distances neither too large to break the absorption continuity nor too small to be indistinguishable. However, the above choices are based on single MIM resonators, and there should be a small deviation when stacking them together. After moderately adjusting the dielectrics' thicknesses, the broadband multilayer MIM resonator, i.e., the unit 2, is constructed in Fig. 3(a). The absorption of unit 2 in Fig. 3(b) shows four distinct peaks with the bandwidth reached 4.7 μm (of absorption intensity above 0.8, ranging from 8.3 μm to 13.0 μm). The low absorption in the range of 5–8 μm indicates the good selectivity of absorption. In Fig. 3(c), EM field images in the *XOZ* plane prove that the magnetic resonance modes are responsible for these four MRA bands. Clearly, the absorption peaks of MRA1, MRA2, MRA3 and MRA4 are generated by the MIM unit of MgF_2, MgO, Y_2O_3 and ZnS, respectively. All of these four resonance modes are well isolated by the metal boundaries between the neighboring dielectric layers. Hence, the stacking of MIM resonator provides a convenience method in MMA design.

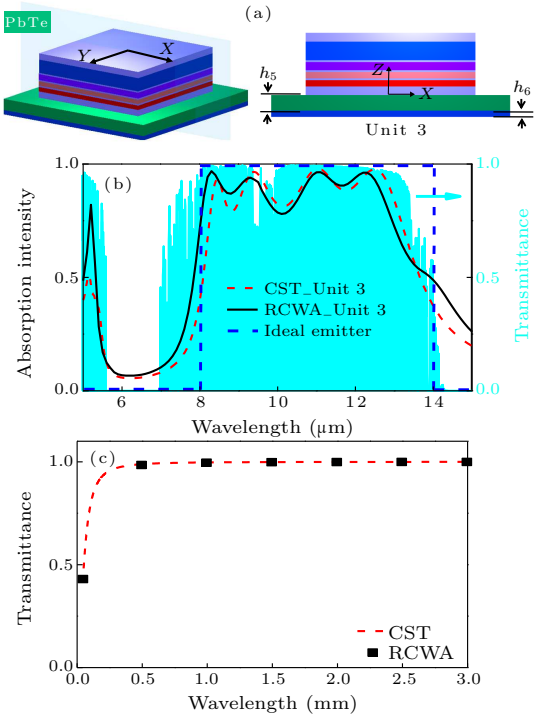

Fig. 4. (a) Schematic of the optimized resonator unit 3, the substrate is replaced by PbTe (thickness of h_5 = 0.25 μm)/MgF_2 (thickness of h_6 = 0.1 μm) bilayer. (b) Comparison of absorption spectra between unit 3 and the ideal emitter. The blue region shows the transmittance of the atmosphere at a temperature of 298.15 K.[40] (c) The microwave transmittance of unit 3.

Wireless communication technologies (especially millimeter-wave and microwave), are widely used in scientific research, industrial manufacturing and also daily life. Hence, in many scenes of thermal emission managements the requirement of thermal radiation compatible with wireless communication should be met. As for traditional MIM, e.g., unit 2, the reliance on the continuous metal substrate results in the disadvantage of wireless signal shielding. To break this limit, we propose to exploit the dielectric substrate for MIM units. Figure 4(a) depicts the schematic of unit 3 with PbTe/MgF_2 bilayer dielectric substrate. In Fig. 4(b), the absorption spectra of unit 3 at normal incidence shows a broadband absorption (8.3–13.1 μm, with absorption intensity over 0.8) resembling to the ideal emitter. There exists only two weak reduction of absorption intensity at 10.1 μm and 11.7 μm as compared with unit 2, which indicates the equivalence of the PbTe/MgF_2 dielectric reflector to the Al metallic reflector. Meanwhile, this bilayer dielectric substrate has been proved to be an effective scheme for wireless signal transparency [shown in Fig. 4(c)]. Thus, the defect of wireless signal shielding for the previous MIM-based radiative coolers[17,41–43] is solved. This design method is also working for electromagnetic stealth scenes where the compatible between infrared and microwave absorbing materials is required.

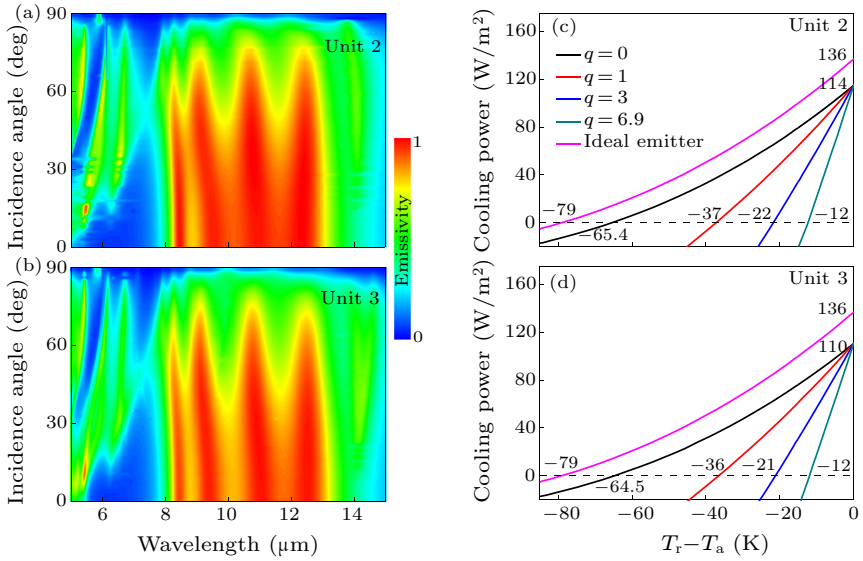

Fig. 5. The angular-dependent absorption (emissivity) of (a) unit 2 and (b) unit 3. The emissivity spectra are obtained by averaging the TE- and TM-polarized absorptivity. Calculated cooling power of (c) unit 2 and (d) unit 3 at nighttime. The factor q represents the non-radiative heat exchange in units of $W \cdot m^{-2} \cdot K^{-1}$.

The angle-dependent emissivity (absorption) diagram is crucial for passive radiative coolers. In Figs. 5(a) and 5(b), we present the comparison between unit 2 and unit 3. It is evident that the thermal emissivity spectra of these two units are stable until the emission angle increases to 50°. Afterwards, the emission bandwidth and intensity of these two units all decline. Note that the emission intensity of unit 3 around the wavelengths of 10.1 μm and 11.7 μm is lower than that of unit 2. This is mainly due to the comparatively lower reflectance intensity of the dielectric substrate in comparison with metal substrate of Al

in unit 2. However, this reduction of emission has very limited impact on the passive radiative cooling performance of unit 3. To evaluate the radiative cooling ability, net cooling power $P_{\rm net}$ of the MMA at nighttime can be expressed by $P_{\rm net} = P_{\rm rad} - P_{\rm abs} - P_{\rm nr}$, where $P_{\rm rad}$ is the radiative power emitted by passive radiative coolers, $P_{\rm abs}$ means the power of incident thermal radiation absorbed by the emitter from ambient atmosphere, and $P_{\rm nr}$ is considered as the power absorbed from other heat transfer patterns except for the radiative mode. The first two terms are closely linked to the black-body radiation,[3] while the last term can be expressed as $P_{\rm nr} = q(T_{\rm a} - T_{\rm r})$ (with the non-radiative heat exchange coefficient $q = q_{\rm cond} + q_{\rm conv}$ containing the contribution from both thermal conduction and conversion). Usually, the value of q is within the range of 1.0–6.9 $\rm W{\cdot}m^{-2}{\cdot}K^{-1}$. Figures 5(b) and 5(c) show the numerically calculated net cooling power of unit 2 and unit 3. Here, the maximum cooling power is obtained for the case in which $T_{\rm r}$ (the temperature of the emitters) is equal to the ambient air temperature $T_{\rm a}$. It shows that unit 3 has a cooling power of 110 $\rm W/m^2$ with only 4 $\rm W/m^2$ below that of unit 2. Meanwhile, as $T_{\rm r}$ decreases gradually and approaches to a steady constant value, the cooling power finally drops to zero. Regardless of the non-radiative heat exchange (or $q = 0$), unit 3 reaches a limited temperature of −64.5 K below $T_{\rm a}$, and is only 0.9 K higher than that of unit 2, as can be seen in Figs. 5(c) and 5(d). What's more, under the opposite condition ($q = 6.9\,\rm W{\cdot}m^{-2}{\cdot}K^{-1}$), a stabilized value of temperature reduction, i.e., −12 K, can be realized for both units 2 and 3. The effect of emissivity spectra difference among these two units is therefore negligible, which proves the effectiveness of our PbTe/MgF_2 dielectric substrate design. Moreover, the theoretical cooling ability of our radiative cooler exhibits the comparable effect as the previous reports.[19,35,44]

In summary, we have proposed a novel broadband MMA based on four stacking MIM units for passive radiation cooling. The optimized absorber has the relative bandwidth of 45% in 8.3–13.1 μm with the absorption intensity over 0.8 in a wide incident angle range (0–50°), which predicts a cooling effect of 12 K below ambient air temperature at nighttime. Compared with the MIM-based passive radiative coolers reported previously, the replacement of continuous Al substrate with PbTe/MgF_2 bilayer dielectric film leads to the transparency window (nearly 100%) for millimeter-waves of wavelengths above 1 mm, while it has little influence on the absorption spectrum in infrared region. Overall, the structure we designed is compatible with silicon-based integrated systems, and thus can be applied for potential applications in the thermal control of integrated devices. Further, the advantage of ultrathin thickness in our design may also promote the miniaturization of photoelectric devices.[45,46]

References

[1] Zhao B, Hu M, Ao X, Chen N and Pei G 2019 *Appl. Energy* **236** 489
[2] Li W and Fan S 2018 *Opt. Express* **26** 15995
[3] Zeyghami M, Goswami D Y and Stefanakos E 2018 *Sol. Energy Mater. Sol. Cells* **178** 115
[4] Hossain M M and Gu M 2016 *Adv. Sci.* **3** 1500360
[5] Zhao D, Aili A, Zhai Y, Xu S, Tan G, Yin X and Yang R 2019 *Appl. Phys. Rev.* **6** 021306
[6] Fan S and Raman A 2018 *Natl. Sci. Rev.* **5** 132
[7] Song J, Seo J, Han J, Lee J and Lee B J 2020 *Appl. Phys. Lett.* **117** 094101
[8] Catrysse P B, Song A Y and Fan S 2016 *ACS Photon.* **3** 2420
[9] Wu W, Lin S, Wei M, Huang J, Xu H, Lu Y and Song W 2020 *Sol. Energy Mater. Sol. Cells* **210** 110512
[10] Wu D, Liu C, Xu Z, Liu Y, Yu Z, Yu L, Chen L, Li R, Ma R and Ye H 2018 *Mater. & Des.* **139** 104
[11] Zhai Y, Ma Y, David S N, Zhao D, Lou R, Tan G, Yang R and Yin X 2017 *Science* **355** 1062
[12] Huang Z and Ruan X 2017 *Int. J. Heat Mass Transfer* **104** 890
[13] Gamage S, Kang E S H, Akerlind C, Sardar S, Edberg J, Kariis H, Ederth T, Berggren M and Jonsson M P 2020 *J. Mater. Chem. C* **8** 11687
[14] Yu W, Lu Y, Chen X, Xu H, Shoo J, Chen X, Sun Y, Hao J and Dai N 2019 *Adv. Opt. Mater.* **7** 1900841
[15] Liu X, Chang Q, Yan M, Wang X, Zhang H, Zhou H and Fan T 2020 *Phys. Chem. Chem. Phys.* **22** 13965
[16] Li Y, Li L, Wang F, Ge H, Xie R and An B 2020 *Opt. Mater. Express* **10** 682
[17] Liu D, Xu Y and Xuan Y 2020 *Appl. Opt.* **59** 6861
[18] Shrestha S, Wang Y, Overvig A C, Lu M, Stein A, Dal N L and Yu N 2018 *ACS Photon.* **5** 3526
[19] Zou C, Ren G, Hossain M M, Nirantar S, Withayachumnankul W, Ahmed T, Bhaskaran M, Sriram S, Gu M and Fumeaux C 2017 *Adv. Opt. Mater.* **5** 1700460
[20] Alaee R, Albooyeh M and Rockstuhl C 2017 *J. Phys. D* **50** 503002
[21] Landy N I, Sajuyigbe S, Mock J J, Smith D R and Padilla W J 2008 *Phys. Rev. Lett.* **100** 207402
[22] Yu P, Besteiro L V, Huang Y, Wu J, Fu L, Tan H H, Jagadish C, Wiederrecht G P, Govorov A O and Wang Z 2019 *Adv. Opt. Mater.* **7** 1800995
[23] Watts C M, Liu X and Padilla W J 2012 *Adv. Mater.* **24** OP98
[24] Qu C, Ma S, Hao J, Qiu M, Li X, Xiao S, Miao Z, Dai N, He Q, Sun S and Zhou L 2015 *Phys. Rev. Lett.* **115** 235503
[25] Kim T, Bae J Y, Lee N and Cho H H 2019 *Adv. Funct. Mater.* **29** 1807319
[26] Li W, Guler U, Kinsey N, Naik G V, Boltasseva A, Guan J, Shalaev V M and Kildishev A V 2014 *Adv. Mater.* **26** 7959
[27] Liu N, Mesch M, Weiss T, Hentschel M and Giessen H 2010 *Nano Lett.* **10** 2342
[28] Ustun K and Turhan-Sayan G 2016 *J. Appl. Phys.* **120** 203101
[29] Cui Y, Fung K H, Xu J, Ma H, Jin Y, He S and Fang N X 2012 *Nano Lett.* **12** 1443
[30] Contractor R, D'Aguanno G and Menyuk C 2018 *Opt. Express* **26** 24031
[31] Bossard J A, Lin L, Yun S, Liu L, Werner D H and Mayer T S 2014 *ACS Nano* **8** 1517
[32] Zhang H, Zhang H, Yang J and Liu J 2019 *Opt. Express* **27** 5346

[33] Feng Q, Pu M B, Hu C G and Luo X G 2012 *Opt. Lett.* **37** 2133
[34] Ye D, Wang Z, Xu K, Li H, Huangfu J, Wang Z and Ran L 2013 *Phys. Rev. Lett.* **111** 187402
[35] Hossain M M, Jia B and Gu M 2015 *Adv. Opt. Mater.* **3** 1047
[36] Ordal M A, Bell R J, Alexander R W, J, Long L L and Querry M R 1985 *Appl. Opt.* **24** 4493
[37] Zhou J, Economon E N, Koschny T and Soukoulis C M 2006 *Opt. Lett.* **31** 3620
[38] Li Y, Zhang P, Liu Y, Jiang R, Gong Y, Deng L and Zhou P 2020 *Opt. Commun.* **472** 126015
[39] Zhang N, Zhou P, Cheng D, Weng X, Xie J and Deng L 2013 *Opt. Lett.* **38** 1125
[40] *ITransmission Spectra R , Gemini Observatory* (accessed: August 2020)
[41] Peng L, Liu D and Cheng H 2019 *Sol. Energy Mater. Sol. Cells* **193** 7
[42] Liu X, Starr T, Starr A F and Padilla W J 2010 *Phys. Rev. Lett.* **104** 207403
[43] Hsu P C, Liu C, Song A Y, Zhang Z, Peng Y, Xie J, Liu K, Wu C L, Catrysse P B, Cai L, Zhai S, Majumdar A, Fan S and Cui Y 2017 *Sci. Adv.* **3** e1700895
[44] Chen Z, Zhu L, Raman A and Fan S 2016 *Nat. Commun.* **7** 13729
[45] Lochbaum A, Dorodnyy A, Koch U, Koepfli S M, Volk S, Fedoryshyn Y, Wood V and Leuthold J 2020 *Nano Lett.* **20** 4169
[46] Wei Q, Huang L, Zentgraf T and Wang Y 2020 *Nanophotonics* **9** 987